Rheologica Acta (2020) 59:783–795
https://doi.org/10.1007/s00397-020-01244-2

ORIGINAL CONTRIBUTION

Linear and nonlinear rheology of oil in liquid crystal emulsions

Zhiwei Liu[1] · Kai Yang[1,2] · Wei Yu[1]

Received: 26 May 2020 / Revised: 12 September 2020 / Accepted: 16 September 2020 / Published online: 22 September 2020
© Springer-Verlag GmbH Germany, part of Springer Nature 2020

Abstract

While the majority of experimental and numerical studies focus on yield stress fluids with short-range repulsive interactions, the effect of long-range interaction is rarely known. In this work, we studied the linear and nonlinear rheological behavior of a model oil in nematic liquid crystal emulsions, which exhibit long-range droplet-droplet interaction. The characteristic of long-range interaction, attractive at large droplet separation and repulsive at a small surface distance, was inferred from the morphology and thixotropy of emulsions. We suggested a model accounting for the plateau modulus purely due to the long-range repulsive interaction. We further illustrated that neither the yield stress nor the relaxation time followed a simple power-law scaling with respect to the distance to jamming. The rescaled steady and dynamic flow curves could not collapse on master curves above jamming transition when the long-range and short-range repulsive interactions contribute simultaneously.

Keywords Yield stress fluids · Jamming transition · PDMS/8CB · Free energy model

Introduction

The yield stress fluids (YSFs) are widely encountered in foodstuff, chemical, pharmaceutical, and personal care products (Bonn et al. 2017; Nelson and Ewoldt 2017). A deep understanding of the relationship between yield stress and composition, as well as their flow behaviors, is of fundamental and practical importance (Bonn et al. 2017; Chen et al. 2010; Nelson and Ewoldt 2017). Dispersions of particles with the different softness (such as solid particles, droplets, or bubbles) in another fluid are the typical approach to prepare yield stress fluids (Vlassopoulos and Cloitre 2014). The physical origin of yield stress has been widely investigated, and the inter-particle interactions are critical for the emergence of apparent yield stress. In the hard-sphere limit, apparent yield stress can appear due to the colloidal glass transition when the thermal motion of colloidal particles is dynamically arrested at packing fraction above ϕ_G (~0.58) (Petekidis et al. 2004; Pusey and van Megen 1986). The relevant stress scale for the yield stress is the Brownian stress, $\sigma_T = k_B T/a^3$ with k_B is the Boltzmann constant, T is the temperature, and a is the particle diameter. In the case of short-range repulsive interactions, a liquid-solid transition takes place at the geometric jamming concentration ϕ_J near the random close packing fraction (~0.64) (Liu and Nagel 2010; Mason et al. 1995; Paredes et al. 2013). The relevant stress scale for the yield stress is $\sigma_0 = \varepsilon/a^3$ with ε is the constant energy scale governing the mechanical property of particles. When there are short-ranged attractive interactions, percolating particle network formed at fraction far below ϕ_G for colloidal particles (such as colloidal glass and colloidal gel (Berthier and Biroli 2011; Berthier and Tarjus 2009; Berthier and Tarjus 2011)) or far below ϕ_J for non-colloidal particles (such as pendular suspension (Chaudhuri et al. 2012; Hao and Yu 2019)) confers the elasticity of the material and results in apparent yield stress. The yield stress of attractive systems is not well-defined because of the thixotropy induced by the inter-particle attractions (Bécu et al. 2006; Fall et al. 2010; Moller et al. 2009). In most studies, the interactions are short-ranged, while little is known about the effect of long-range (surface distance in the same order of non-colloidal particles size) interactions on the yield stress.

Electronic supplementary material The online version of this article (https://doi.org/10.1007/s00397-020-01244-2) contains supplementary material, which is available to authorized users.

✉ Wei Yu
wyu@sjtu.edu.cn

[1] Advanced Rheology Institute, Frontiers Science Center for Transformative Molecules, State Key Laboratory for Metal Matrix Composite Materials, Department of Polymer Science and Engineering, Shanghai Jiao Tong University, Shanghai 200240, People's Republic of China

[2] Malvern Instruments, Shanghai, China

For the non-colloidal system with short-ranged repulsive interactions, some simple scaling features near the jamming transition have been found. In the jammed regime, the yield stress is found to obey the power-law $\sigma_y \sim |\Delta\phi|^{\Delta}$ (Ikeda et al. 2013; Kawasaki et al. 2015; Olsson and Teitel 2007; Paredes et al. 2013), where $|\Delta\phi| = |\phi - \phi_J|$ is the distance to ϕ_J. The prerequisite of such power law is that the energy scale ε for the interaction is a constant, which is independent of the packing fraction. Meanwhile, the characteristic yielding time, defined in the Herschel-Bulkley (HB) equation $\sigma = \sigma_y \left(1 + \left(\lambda\dot{\gamma}\right)^n\right)$, is found to obey a similar power law with a different exponent, $\lambda \sim |\Delta\phi|^{-\Gamma}$ (Basu et al. 2014; Dekker et al. 2018; Dinkgreve et al. 2015, 2018; Nordstrom et al. 2010; Paredes et al. 2013). Based on these scaling relations, the steady flow curves above ϕ_J collapse onto a master curve by rescaling $\sigma/|\Delta\phi|^{\Delta}$ versus $\frac{\dot{\gamma}}{|\Delta\phi|^{\Gamma}}$ (Basu et al. 2014; Dekker et al. 2018; Dinkgreve et al. 2015, 2018; Nordstrom et al. 2010; Olsson and Teitel 2007; Paredes et al. 2013). Such a phenomenon has been observed for athermal emulsions with mobile, rigid, and softer electrostatic surfactants (Dinkgreve et al. 2015, 2018), and foams (Dinkgreve et al. 2015), and even for thermal emulsions and suspension (Dinkgreve et al. 2018). For jamming microgel system (Dinkgreve et al. 2015), it is hard to justify the above scaling laws due to the difficulty of quantifying the packing fraction, but the collapsed flow curve can still be obtained by rescaling σ/σ_y versus $\lambda\dot{\gamma}$. However, it is unclear whether the power-law scaling is the necessary condition of the collapse of flow curves. Recent simulations (Irani et al. 2014, 2016), incorporating a weak attractive interaction beyond the soft repulsive interaction, illustrated different scaling laws in attraction dominated regime and repulsion dominated regime, thus results in the failure of the collapse of flow curves. These results indicate the non-universality of the jamming transition when multiple interactions are effective. However, it has not been observed in experiments.

The question we ask here is whether long-range interaction can lead to the apparent yield stress, and if so, how the jamming transition is affected by the simultaneous presence of the long-range and short-range repulsive interactions. Long-ranged repulsive interaction is considered instead of the attractive interaction adopted in simulations (Irani et al. 2014, 2016), because aggregation due to attraction would induce thixotropy and complicate the problem (Bécu et al. 2006; Fall et al. 2010; Moller et al. 2009). Such systems with short-ranged and long-ranged repulsive interactions are the best model systems to study the role of multiple interactions on the jamming phenomenon.

It has been reported that a colloidal gel can form by dispersing colloidal particles in a liquid crystal (Anderson et al. 2001; Bukusoglu et al. 2014; Meeker et al. 2000; Wood et al. 2011; Zapotocky et al. 1999). Different routes had been suggested to gelation colloids in liquid crystal. In the first route, gelation happens during cooling the colloids/liquid crystal suspension from the isotropic state of liquid crystal, where the formation of the percolating colloidal network can happen either after the nucleation and growth of nematic domains (Meeker et al. 2000) or before it (Bukusoglu et al. 2014). In the second route, gelation happens when dispersing colloids in the nematic state of liquid crystal by mechanical shearing (Wood et al. 2011), where the entanglement of topological line defects around colloids in the liquid crystal leads to a percolated network of colloids. In this work, we use an emulsion containing continuous liquid crystal phase (He et al. 2012; Yang et al. 2018; Yang and Yu 2017) as our experimental system. In contrast to the common water/oil emulsion, where the yield stress is purely ascribed to the jamming of dispersed droplets (Bécu et al. 2006; Fall et al. 2010; Moller et al. 2009; Seth et al. 2011), the topological defects in the liquid crystal around droplets can induce additional long-range interactions between droplets, which leads to the apparent yield stress in emulsions even far below the jamming concentration. The experimental system is used to show how rheological properties below and above ϕ_J scale with respect to the packing fraction and the distance $|\Delta\phi|$ in the presence of multiple repulsive interactions. The scaling exponents above ϕ_J are different from conventional simple emulsions (Dekker et al. 2018; Dinkgreve et al. 2018, 2015; Paredes et al. 2013). Rescaling of both steady flow curves and dynamic flow curves collapses only when there is one repulsive interaction, i.e., below jamming concentration. We propose a simple model to elucidate the relative strength of two repulsive interactions and their roles in the yield transition.

Experimental

PDMS/8CB emulsions

Our experimental systems are dilute and concentrated emulsions of polydimethylsiloxane (PDMS) droplets in the matrix of liquid crystal 4-octyl-4-biphenylcarbonitrile (8CB). 8CB was purchased from Yantai Valiant Fine Chemicals Co. Ltd., China. 8CB presents a crystal-smectic transition at 22 °C, a smectic-nematic transition at 34 °C, and a nematic-isotropic transition at 42 °C (He et al. 2012; Yang et al. 2018; Yang and Yu 2017). Polydimethylsiloxane (PDMS) was purchased from Shanghai Resin Plant, China, without further purification. The weight-average molecular weight of PDMS is about 240,000 g/mol. The density of PDMS and 8CB is 0.98 g/cm^3 and 0.99 g/cm^3 at 25 °C, respectively. The 8CB displays almost no shear-thinning behavior under the tested shear rate at 35 °C (Fig. S1). The shear viscosity of PDMS and 8CB is 155.3 Pa.s and 0.028 P.s at 35 °C, respectively. In this experiment, the volume fractions of PDMS in the blends are from 0.01 to 0.9. 8CB was mixed with PDMS by hand at

25 °C using a spatula in a 50-ml beaker for 5 min, which was proved to be sufficient to make the rheological properties of the mixtures reproducible. Finally, all the blends were placed in a vacuum oven for 48 h at 25 °C to exclude air bubbles before the experiments.

Rheological measurements

All rheological tests were carried out on a Kinexus Ultra rotational rheometer (NETZSCH Instruments) using parallel plates at 35 °C, where 8CB is in the nematic state. The diameter of the parallel plates was 40 mm, and the gap was 0.5 mm. Fine waterproof sandpaper (3 M) was glued to plate surfaces to reduce wall slip (Yang et al. 2018; Yang and Yu 2017). Before carrying out any experiment, samples are kept at 35 °C for 5 min in order to assure the same initial condition for all measurements. First, the steady shear experiments were performed shear rate sweeps from 100 to 0.0001 s^{-1}. Besides, the upward shear rate sweeps with the same protocol were also used to check the thixotropic properties (Divoux et al. 2013; Fall et al. 2010) of PDMS/8CB emulsions. Then, frequency sweep (0.01–100 Hz) under the fixed stress amplitude of 0.5 Pa in the linear viscoelastic regime was selected to obtain the linear viscoelastic data. Furthermore, oscillatory stress amplitude sweeps at 0.1 Hz were carried out in the range from 0.1 to 500 Pa. At each stress amplitude, 20 cycles of raw data of torque and displacement were recorded. The sampling rate was 8192 points for 20 cycles. The last ten cycles were used for further data analysis.

Optical microscopy

A polarizing optical microscope (LEICA DM2500P) equipped with a home-made heating stage temperature control was used to observe the morphology of PDMS/8CB emulsions under cross-polarized field and bright field. The mean droplet radius of PDMS and the distribution of PDMS droplets radius for PDMS/8CB emulsion with different PDMS contents were measured by IMAGE PRO software.

Results and discussion

Solid-like behavior

The steady flow curves of all samples are shown in Fig. 1a. Strikingly, the steady shear stress extrapolates toward non-zero apparent yield stress at vanishing shear rate at PDMS packing fraction as low as 0.10. The solid-like behavior is also observed from the storage modulus in the linear viscoelastic regime (Fig. 2). The terminal behavior is typical for a viscoelastic liquid (G'~ω^2) at PDMS volume fraction about 0.01~0.05. At high concentration (above 0.3), G' shows a plateau while a minimum is seen in G". For PDMS content between 0.15 and 0.30, the minimum in G" is absent while plateau of G' at low frequency is still clear down to frequency 5×10^{-4} Hz. For PDMS content 0.10, there is a broad shoulder in G', which decays to zero at 10^{-3} Hz. Therefore, the solid-like behavior is obvious over a wide range of PDMS content from about 0.15 up to 0.90 in the experimental time scale down to 10^{-3} Hz, which is in contrast with normal emulsions where apparent yield stress appears only above the jamming concentration (Dekker et al. 2018; Dinkgreve et al. 2015; Mason et al. 1995; Paredes et al. 2013; Seth et al. 2011). The appearance of yield stress can be further validated by creep tests (Fig. S2), where the shear rate approaches zero under stress below the yield stress, while approaches a constant non-zero value above the yield stress.

Typical morphologies for emulsions with PDMS content above 0.55 are observed by optical microscopy and shown in Fig. 1b. The morphology of PDMS/8CB emulsions is droplet-in-matrix with micron-scale droplet size. The radius of PDMS droplets over the whole range of PDMS is measured and shown in Fig. S3. The mean radius of PDMS droplet decreases as the PDMS content increases. Polydispersity is relatively narrow for PDMS content higher than 0.6 (Fig. S4). The polydispersity in size also prevents the droplet from crystallizing (Cohen-Addad and Hohler 2014; Joshi 2014; Lu and Weitz 2013; Pusey 2008; Seth et al. 2011; Vlassopoulos and Cloitre 2014). At high PDMS content (above the random close packing fraction $\phi_{RCP} \approx 0.64$), the shape of droplets gradually becomes irregular, and PDMS droplets are tightly packed together where the continuous 8CB forms a thin-film between the PDMS droplets. Such morphology is typical for jammed concentrated emulsions stabilized by surfactant (Cohen-Addad and Hohler 2014; Seth et al. 2011) and foams (Cohen-Addad and Hohler 2014; Katgert et al. 2013). In normal emulsions, the apparent yield stress above ϕ_{RCP} has been ascribed to the jamming transition (Dekker et al. 2018; Dinkgreve et al. 2015; Mason et al. 1995; Paredes et al. 2013; Seth et al. 2011), but the jamming transition cannot explain the emergence of yield stress and non-zero plateau in storage modulus below 0.60, where fluid-like behavior with finite viscosity is observed for normal emulsions (Dinkgreve et al. 2018, 2015; Paredes et al. 2013).

Scaling behavior

Firstly, we use the HB model $\sigma = \sigma_y\left(1 + \left(\tau\dot{\gamma}\right)^{\beta}\right)$ to fit the flow curves of PDMS/8CB emulsions, as shown in Fig. S5. Although the HB model works well for $\phi > \phi_{RCP}$, the HB model displays an obvious deviation from the experimental data below ϕ_{RCP}, especially at the lower shear rate region. To obtain the satisfactory fit, the HB model was modified in the spirit of the Carreau-Yasuda model (Boyd et al. 2007) for shear-thinning behavior of the non-Newtonian fluid, $\sigma = \sigma_y$

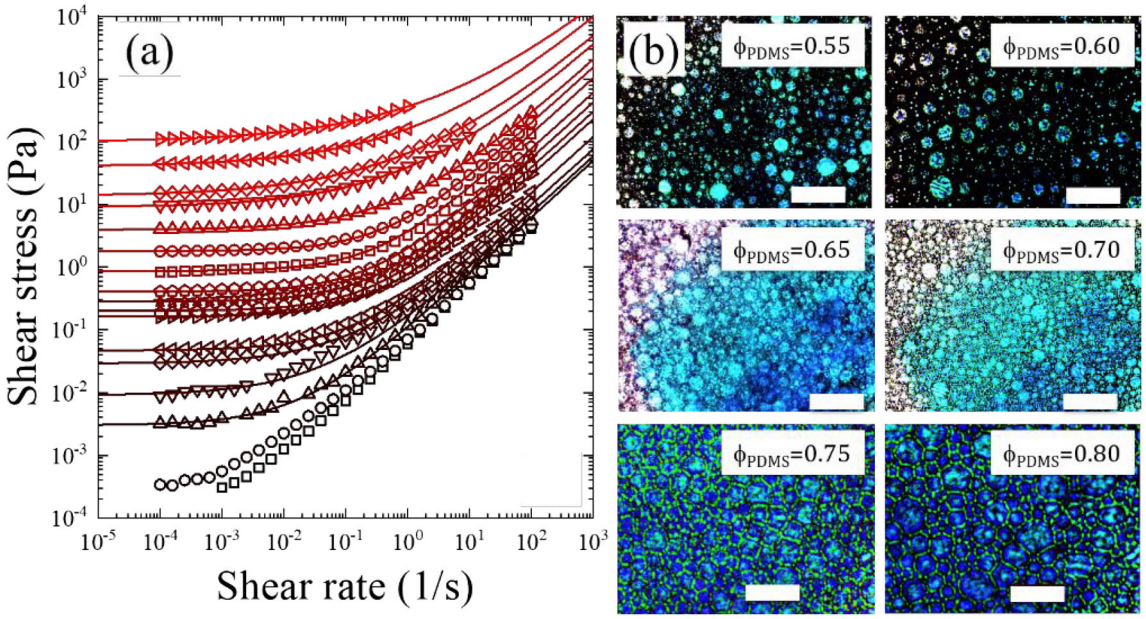

Fig. 1 Steady flow curves (**a**) and images from optical microscopy (**b**) of PDMS/8CB emulsions. In (**a**), the PDMS contents from bottom to top are 0.01, 0.05, 0.10, 0.15, 0.20, 0.30, 0.40, 0.45, 0.50, 0.55, 0.60, 0.65, 0.70, 0.75, 0.80, 0.85, and 0.90. Solid lines in (**a**) are the fitting curves of the modified HB model with constant value 0.9 for *m*. The scale bars in (**b**) represent 10 μm

$\left(1+\left(\tau\dot{\gamma}\right)^{n}\right)^{m}$, with additional exponent m. The fitting curves are shown in Fig. 1a, and the fitting results are greatly improved with a constant value m = 0.9. The dependence of the apparent yield stress σ_y and the plateau modulus of G' at the low frequency on PDMS content is shown in Fig. 3a. The apparent yield stress and plateau modulus increase monotonically with PDMS content, and both exhibit power-law dependence on the PDMS content with a similar power-law exponent. The power-law exponent increases from about 2.90 to about 11.0, and the transition appears near 0.60, which is close to ϕ_{RCP}. The dependence of characteristic time τ on PDMS content is shown in Fig. 3b. Three regions are seen, where τ decreases with PDMS content when it is below about 0.20 or above about 0.60, while keeps constant between 0.20 and 0.60.

One distinct feature in Fig. 3 is the appearance of apparent yield stress below ϕ_{RCP}. The solid-like behavior in emulsions with droplets concentration far below the jamming concentration has also been observed in charge-stabilized nanoemulsions (Kim et al. 2016; Scheffold et al. 2014; Wilking and Mason 2007), where the screen-charge electrostatic repulsion between droplets accounts for the elastic

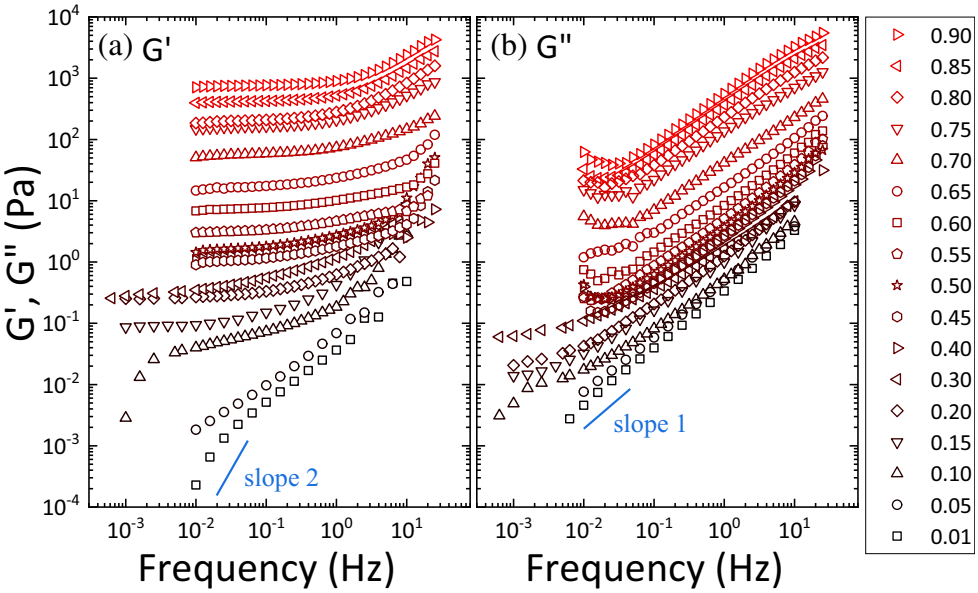

Fig. 2 Storage modulus (**a**) and loss modulus (**b**) of PDMS/8CB emulsions with different PDMS contents

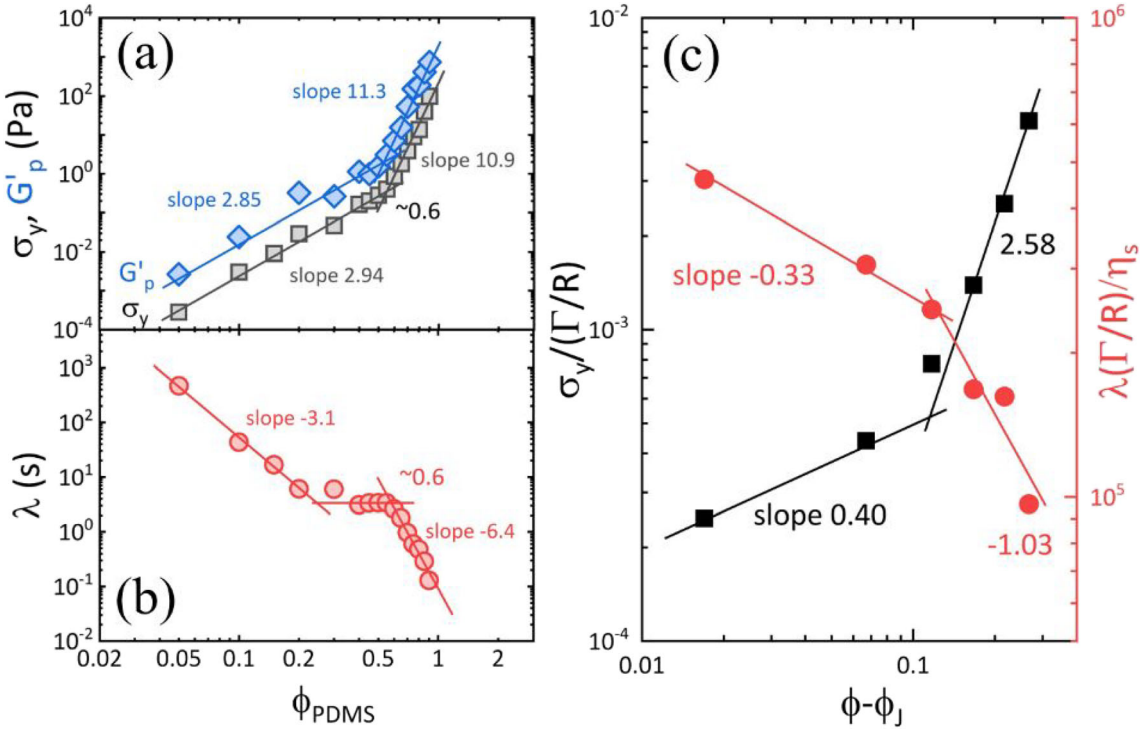

Fig. 3 Yield stress and plateau modulus (**a**), and characteristic time (**b**) of PDMS/8CB emulsion as a function of PDMS content. **c** Reduced yield stress and characteristic time as a function of relative concentration. Γ is the interfacial tension, R is the droplet radius, η_s is the viscosity of continuous phase (8CB), ϕ_J is the jamming concentration ($\phi_J \approx \phi_{RCP}$)

behavior. The Debye screening length is typically smaller than 4 nm (Kim et al. 2016; Scheffold et al. 2014; Wilking and Mason 2007), indicating the interaction distance is at most tens of nanometer because of the exponential dependence of the repulsive force on the inter-droplets surface distance. Therefore, the solid-like behavior at low volume fraction due to electrostatic repulsion would only be possible for nano-scale droplets (Kim et al. 2016). In PDMS/8CB emulsion, the inter-droplets surface distance between non-colloidal disordered droplets at low PDMS content ($\phi < 0.60$) is much larger, varying from about 20 μm for $\phi = 0.1$ to about 0.6 μm for $\phi = 0.6$, as estimated by $h = 2R\phi_J^{1/3}\left(\phi^{-1/3}-1\right)$ (Kim et al. 2016). The emergence of apparent yield stress in dilute PDMS/8CB emulsions should be ascribed to certain long-ranged (micron-scale) inter-droplets interactions, which decays much slower than the exponential function. The solid-like behavior of PDMS/8CB emulsion for $\phi < \phi_{RCP}$ can also be observed in the smectic state of 8CB (He et al. 2012), but the emulsions turn into liquid-like in isotropic state of 8CB (see Fig. S6), which indicates the long-range interaction originates from the nematic (or smectic) state of liquid crystal. Actually, the solid-like behavior has also been reported in the colloids/LC system when the particle concentration is far below that required for glass transition (Wood et al. 2011). A power-law dependence of the plateau modulus on the particle concentration is observed in polymethylmethacrylate (PMMA) colloidal particles/4-cyanobiphenyl (5CB) system with exponent about 2.5 ± 0.5 (Wood et al. 2011). The power-law exponent for PDMS/8CB emulsion lies well in this range. However, the value of plateau modulus in PDMS/8CB emulsion is only about 10^0 Pa at PDMS volume fraction 0.50, much smaller than that ($\sim 10^4$ Pa) in PMMA colloids/5CB gel at the similar volume fraction of PMMA particles. Wood et al. (Wood et al. 2011) had ascribed the elasticity of PMMA colloids/5CB gel to the Frank elastic energy over a distance on the order of a disclination core (l_c) about 5 nm. Because the Frank elastic stress is proportional to the reciprocal of the square of defect length, four orders lower of the plateau modulus in PDMS/8CB than PMMA/5CB indicate the defect length in PDMS/8CB system is about 100 larger, which is be about 500 nm. Such length is close to the average surface distance between PDMS droplets at $\phi = 0.6$.

We now ask if the long-range interaction affects the power laws as observed for yield stress and characteristic time near the vicinity above the jamming concentration for simple jamming systems. The first thing is how the jamming concentration can be determined in PDMS/8CB emulsions, which is not so easy or straightforward as those simple emulsions. In simple emulsions, the appearance of yield stress (Dinkgreve et al. 2018; Paredes et al. 2013), the dependence of yield stress on concentration (by Princen model or other similar models) (Cohen-Addad and Hohler 2014; Mason et al. 1995), or the morphology (Cohen-Addad and Hohler 2014) can be used to quantify the jamming concentration. The method using the

appearance of yield stress is not applicable in our case because the yield stress appears far below the usual jamming concentration, where only a transition of concentration dependence is seen near $\phi \approx 0.6$. The method using the dependence of yield stress on concentration by fitting the Princen model might work, but the yield stress in such a model is purely ascribed to the interfacial tension, which is also not the case in the present system. The method using images from optical microscopy indicates the deformation of droplets into irregular shapes above $\phi = 0.6$ (Fig. 1), which is the characteristic of jamming in an emulsion, but the critical point is difficult to quantify from images. Therefore, the random close packing concentration is used as the jamming concentration, $\phi_J = \phi_{RCP}$.

We plot the normalized apparent yield stress and the normalized relaxation time with the distance to jamming transition ($\Delta\phi = \phi - \phi_J$) in Fig. 3c. In contrast to the simple jamming systems (Dekker et al. 2018; Dinkgreve et al. 2018; Dinkgreve et al. 2015; Paredes et al. 2013), neither the yield stress nor the relaxation time of PDMS/8CB emulsions shows a simple power-law scaling. Actual, the power-law exponent Δ of yield stress changes from about 0.4 at low $\Delta\phi$ to 2.58 at higher $\Delta\phi$, and the exponent Γ for the normalized relaxation time varies from 0.33 to 1.03. These exponents of PDMS/8CB emulsions are different from the results reported in glass transition for Brownian suspensions or a jamming transition for non-Brownian systems(Dekker et al. 2018; Dinkgreve et al. 2018, 2015; Nordstrom et al. 2010; Paredes et al. 2013), i.e., $\Delta \approx 2$ and $\Gamma \approx 4$. Both the change of the scaling exponents with $\Delta\phi$ and the deviation of the exponents from those of normal emulsions imply that the simple power-law scaling is not the universal character of jamming transition. Instead, it would be the universal character of jamming transition in systems with only short-ranged repulsive interaction.

Long-range interaction

When a particle or droplet is immersed in a liquid crystal medium, the competition of the bulk elastic and surface anchoring energies determines the type of elastic multipoles under suitable surface boundary conditions (Smalyukh 2018). When two particles get close to one another, the superposition of elastic distortions induced by the interacting particles leads to the potential energy of elastic interaction between nematic colloidal multipoles. The elastic interaction can be repulsive or attractive, depending on the type of multipoles (Smalyukh 2018). The interaction between a pair hexadecapoles depends on the relative position of two particles (Senyuk et al. 2016; Smalyukh 2018). The interaction between a pair of quadrupoles is attractive, which results in the entanglement of the defect ring near the particle (Humpert et al. 2018; Wood et al. 2011). The most frequently encountered dipole-dipole interaction can be attractive as well as repulsive (Smalyukh et al. 2004). The attraction is found with the inter-droplet attractive force proportional to $K(a/r)^4$ with r the center distance between two droplets (Poulin et al. 1997). However, the attractive interaction quickly turns to strong repulsive interaction as $r \sim 3a$ (Poulin et al. 1997). Such inter-droplet separation corresponds to the volume fraction of about 0.07~0.16, depending on whether the random distribution or simple cubic distribution of droplets is used to estimate the inter-droplet separation. It implies that PDMS droplets in the 8CB matrix would experience strong repulsive interaction at PDMS content above 0.07~0.16 because of the small inter-droplet separation. Such concentration is also the critical concentration above which evident solid-like behavior is observed from linear viscoelasticity.

The scenario described above indicates that the interactions between PDMS droplets in a nematic matrix (8CB) depend on the droplet concentration. The inter-droplet center distance is sufficiently large at low concentration (below 0.07~0.16) to induce attractive interaction and cause aggregation of droplets, which can be observed from optical microscopy under both cross-polarized field and bright field (Fig. 4). Liquid crystal (the light area under cross-polarized field) is the continuous phase, and PDMS is the dispersed phase. Aggregation of small PDMS droplets is clear for 5% and 10% emulsions, which results from the attractive interaction between droplets. However, aggregated droplets are stable without obvious coarsening, implying the repulsive interaction between droplets at separation about droplet size. For emulsions with PDMS above 20%, no evident aggregation is seen, although the droplet size distribution is clear. The inter-droplet surface distance is about the same size as the small droplets, which is the repulsive dominant region, as also observed by Poulin et al. (Poulin et al. 1997)

Therefore, we would regard the "long-range" interaction repulsive in PDMS/8CB emulsion with PDMS content above 0.07~0.16. It should be noted that the "long-range" here is compared with the thickness of films in compressed emulsion above jamming. The former can be as large as the droplet size, while the latter is normally below 1/10 of the droplet size. In contrast, the "long-range" interaction is attractive in dilute emulsions when PDMS content is below 0.07~0.16.

In addition to the morphology, which indicates the interactions between droplets, the thixotropy of emulsions can also serve as supporting evidence for the type of interaction. Attractive emulsions exhibit strong thixotropy (Bécu et al. 2006; Fall et al. 2010; Moller et al. 2009), while repulsive emulsions are usually simple yield stress fluids with weak/no thixotropy (Bécu et al. 2006; Fall et al. 2010; Moller et al. 2009; Paredes et al. 2013). PDMS/8CB emulsions with different PDMS contents are tested by shear rate downward sweep and upward sweep experiments with a duration 60 s at each shear rate. As shown in Fig. 5, PDMS/8CB emulsions exhibit no thixotropy for PDMS content as low as 0.20 due to

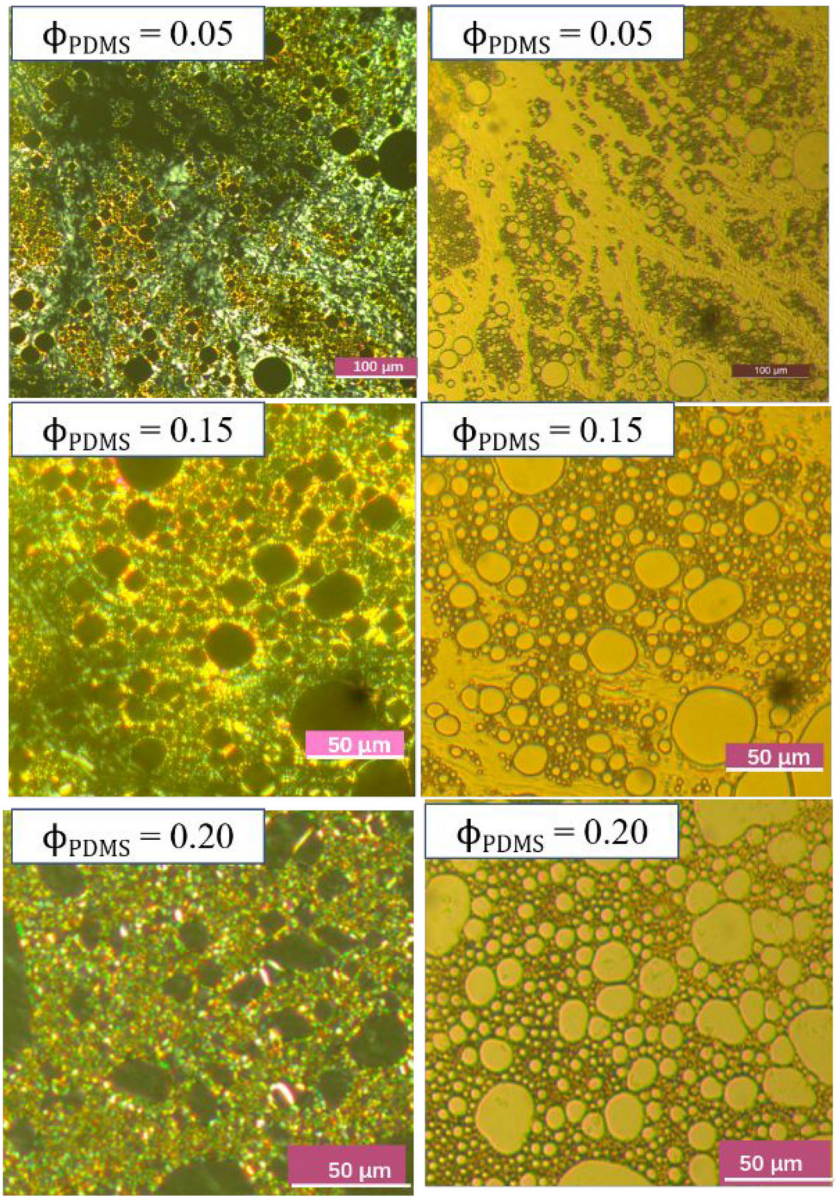

Fig. 4 Optical micrograph of PDMS/8CB emulsions with different PDMS contents under cross-polarized field (left column) and bright field (right column)

the superposition of the downward sweep curve and upward sweep curve. No thixotropy also implies that the interactions are dominated by repulsive interaction, which is consistent with the morphology observation (Fig. 4). We also test for the time evolution of the storage and viscous moduli of PDMS/8CB with 30% PDMS over 1 h after pre-shear in Fig. S7. The storage and viscous modulus almost keep constant even after a long time, which indicates the sample has no aging or thixotropic effects (Koumakis and Petekidis 2011; Lidon et al. 2017). It implies again the dominant interaction at this composition (30% PDMS) is repulsive. This phenomenon is in contrast with that in the PMMA/5CB system, where the recovery of modulus takes several hundreds of seconds (Wood et al. 2011), and the strong thixotropy was ascribed to the attractive interaction in their system.

Model for plateau modulus

We now ask if the solid-like behavior can be quantitatively correlated to the long-range interaction. Because of the disappearance of the solid-like behavior of PDMS/8CB emulsions in the isotropic state of 8CB, the long-range interaction must be related to the nematic properties of liquid crystal. We adopted an energetic approach to model the linear elastic shear modulus $G_p^{'}$ of PDMS/8CB emulsion. In this approach, the free energy of emulsion is composed of the entropic part (F_{ent}), the interfacial part (F_{int}), and the Frank elastic part (F_{LC}). Mason et al. (Mason and Scheffold 2014) had suggested the entropic contribution and the interfacial contribution per droplet as $f_{ent} = F_{ent}/N = -3k_BT\ln(\phi_J + \phi_d - \phi - \alpha\gamma^2)$, and $f_{\mathrm{int}} = F_{\mathrm{int}}/N = 4\pi\xi\Gamma R^2\phi_d^2$, where N is the

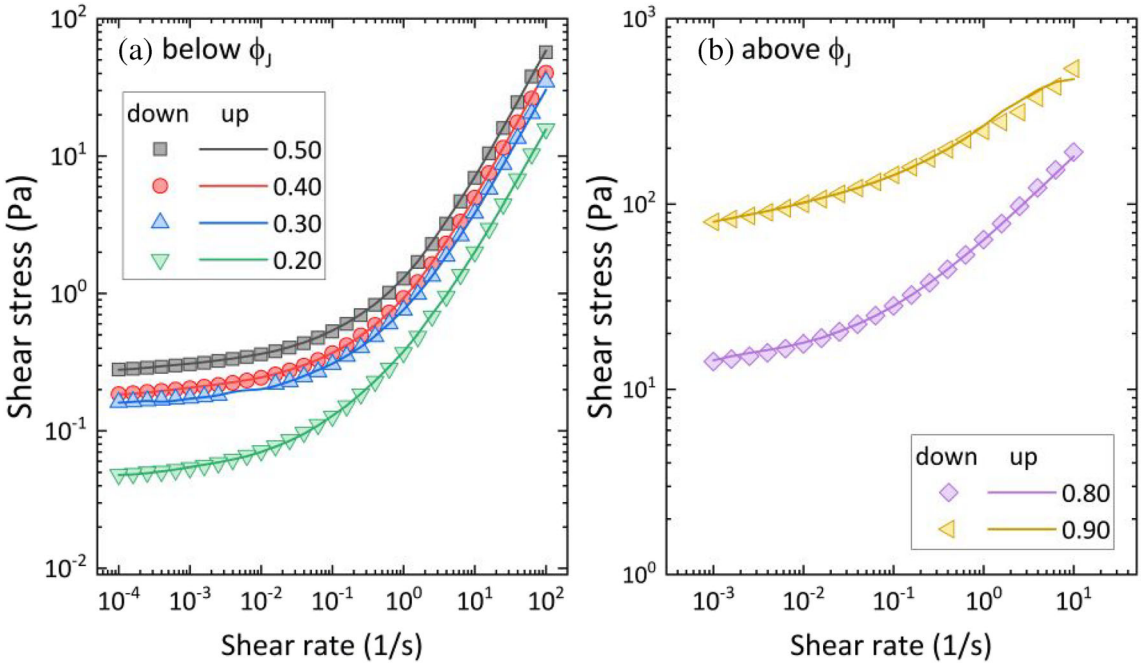

Fig. 5 Thixotropy loop of PDMS/8CB emulsions with different PDMS contents. The duration at each shear rate is 60 s

number of droplets per volume, k_B is the Boltzmann constant, T is the temperature, and γ is the strain. ξ is a fitting parameter related to the distribution of facet sizes and local neighbor configurations, and $\alpha\gamma^2$ denotes the change of positional configurations and reduction of the translational free volume fraction due to weak shear deformation, where α is a dimensionless parameter. ϕ_d represents an upward shift of jamming concentration due to slight deformation of spherical droplets, which can be determined by minimizing the free energy: $\partial(F_{ent}+F_{\mathrm{int}})/\partial\phi_d|_{\phi_d=\phi_d^*}=0$ (Mason and Scheffold 2014). Then, the plateau modulus can be obtained from the second derivative of free energy with droplet volume fraction (Mason and Scheffold 2014),

$$G'_{\mathrm{int}}=\frac{\phi}{NV_{drop}}\frac{\partial^2(F_{\mathrm{int}}+F_{ent})}{\partial\gamma^2}\bigg|_{\phi_d=\phi_d^*,\gamma=0}$$
$$=6\alpha\xi\frac{\Gamma}{a}\phi\left[(\phi-\phi_J)+\sqrt{(\phi-\phi_J)^2+\phi_T^2}\right] \quad (1)$$

with $\phi_T^2=(3k_BT)/(2\pi a^2\xi\Gamma)$. Satisfactory fit has been found for the plateau modulus of the oil-water emulsion by Eq. (1) (Mason and Scheffold 2014). The incorporation of the entropic contribution results in a non-zero plateau modulus even below ϕ_J. However, the plateau modulus drops over two decades in a narrow regime ($\sim\phi_T$) below ϕ_J, which is not the reason for the plateau modulus of PDMS/8CB below ϕ_J.

The main difference between PDMS/8CB emulsion and the oil-water emulsion is that the continuous fluid is in the nematic state in PDMS/8CB emulsion. According to the Frank-Oseen theory (Frank 1958), spatial variations in the director field (**n**) of nematic liquid crystal may disrupt the molecular packing and produce excess free energy density, which is proportional to the Frank elastic constant K and quadratic of director gradient $\nabla\mathbf{n}:(\nabla\mathbf{n})^T$ under the one-constant approximation. The distance over which the director changes may be as small as a molecular length scale, or as large as the average distance between line disclinations (Frank 1958). In the bulk of a nematic liquid crystal, disclination lines are energetically disfavored, which will shrink in length and annihilate one another until they disappear completely because of the Frank stress. However, in PDMS/8CB emulsion, the disclination lines will be pinned by the anchoring conditions (Chuang et al. 1991) at the interface of PDMS/8CB. As a result, the Frank elasticity contribution to the free energy per volume should be proportional to K/h^2, where h is the average surface distance between PDMS droplets. Therefore, the Frank elastic energy per droplet in PDMS/8CB emulsion can be expressed as $f_{LC}=F_{LC}/N=4\pi R^2h\beta K/h^2$, where the volume of matrix around a droplet is estimated by the product of the surface area of a droplet $4\pi R^2$ and half of the average surface distance between droplets $h/2$. Considering the change surface distance between two droplets due to the surface curvature, βh is taken as the effective average surface distance with β a fitting parameter, which would be close to 0.5. f_{LC} is inversely proportional to the inter-droplet surface distance, manifesting the character of long-range interaction. The surface distance is given by $h=2a\phi_J^{1/3}\left(\phi^{-1/3}-(1-\alpha\gamma^2)^{-1/3}\right)$ (Kim et al. 2016). Then, the plateau shear modulus due to the Frank elasticity of nematic liquid crystal can be obtained as

$$G'_{LC} = \frac{\phi}{NV_{drop}} \frac{\partial^2 F_{LC}}{\partial \gamma^2}\bigg|_{\phi_d=\phi_d^*,\gamma=0} = \frac{K\alpha\beta\phi^{5/3}}{a^2\left(1-\phi^{1/3}\right)^2\phi_J^{1/3}} \quad (2)$$

We compare the plateau modulus from the above model $G'_p = G'_{\text{int}} + G'_{LC}$ with the experimental data of PDMS/8CB emulsions in Fig. 6a. The plateau values of the elastic shear modulus G'_p are determined at the lower frequency regions, as shown in Fig. 2. The agreement in the whole range of PDMS content is satisfactory. The results show that G'_{LC} dominates below ϕ_J, while both G'_{int} and G'_{LC} contribute above ϕ_J. It is also seen from the inset of Fig. 6a that the ratio G'_{int}/G'_{LC} is not a monotonic function of PDMS content. The maximum of G'_{int}/G'_{LC} coincides with the change of scaling exponent of apparent yield stress and relaxation time (Fig. 3), which implies the change of scaling exponent of apparent yield stress is ascribed to the change of dominating contribution of elastic property

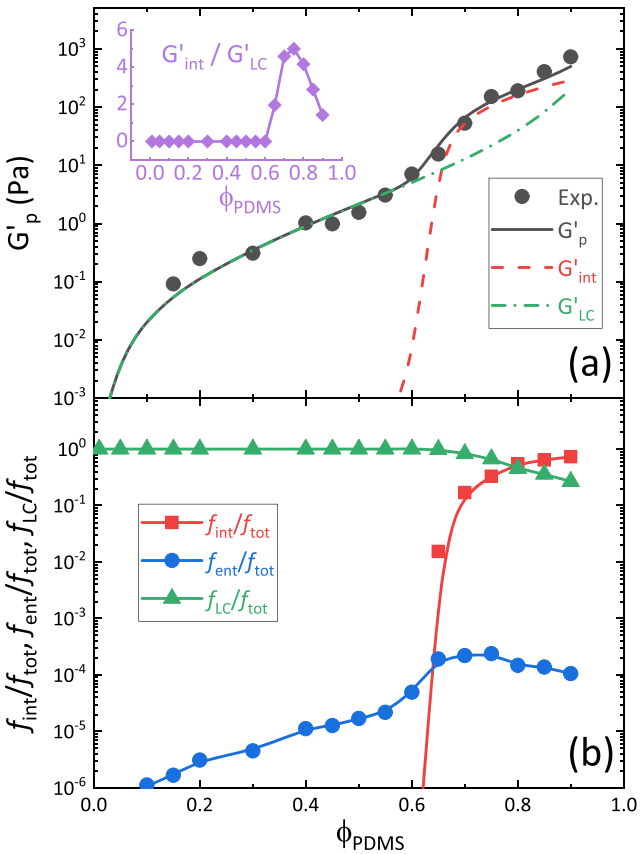

Fig. 6 **a** Plateau modulus of PDMS/8CB emulsion and comparisons between experiments and model predictions. **b** The fraction of free energies as a function of PDMS concentration. The fitting parameters are $R = 3\mu m$, $\Gamma = 6mN/m$ (Wu et al. 2006),$K = 5 \times 10^{-12}N$(He et al. 2012; Zywocinski et al. 2000). $\alpha = 1.0$ and $\xi = 0.05$ are adjustable parameters for the entropic contribution, which are determined by fitting with the plateau modulus above the jamming concentration. The fitting parameter for the Frank elastic part is $\beta = 0.45$, which is determined by fitting with the plateau modulus below jamming concentration

from the interfacial energy in the vicinity of ϕ_J to the Frank elastic energy of 8CB far above ϕ_J. The relative contributions of interfacial (and entropic) and liquid crystal terms to the total free energy f_{tot} are compared in Fig. 6b. Clearly, for $\phi < \phi_J$, the Frank elastic energy dominates in the total free energy, while the interfacial energy increases above ϕ_J and dominates at higher PDMS content. The entropic contribution has been found to be important at the concentration slightly below ϕ_J in water/oil emulsion. However, it is negligible in the whole range of concentration in PDMS/8CB emulsion.

The above analysis is for emulsions with monodispersed droplet size. The polydispersity in droplet size may have two effects on the model predictions. On the one hand, the contribution from the interface (Eq. 1) in the case of polydispersed droplet size can be written as $G'_{\text{int}} = \sum 6\alpha\xi \frac{1}{a_i}\phi_i[(\phi-\phi_J) + \sqrt{(\phi-\phi_J)^2 + \phi_T^2}]$, with ϕ_i the volume fraction of droplet with radius a_i. Such expression is equivalent to Eq. (1) if the harmonic average radius $\phi/\overline{a} = \sum \phi_i/a_i$ is used in Eq. (1). If the volume average radius used in the original fitting is replaced by the harmonic average radius, which is about 0.55~0.7 of R_v above jamming from statistics, the fitting results will not be greatly affected except the fitting parameter ξ in Eq. (1) becomes about 1.6 times the previous value.

On the other hand, the droplet size distribution would also affect the nearest inter-droplets surface distance. Lu and Torquato (Lu and Torquato 1992) suggested a complicated model and illustrated the increase of the nearest inter-droplets surface distance as the polydispersity of particle size increases. Such an effect can be simply regarded as an increase of the jamming concentration (Gam et al. 2012). Santos et al. (2014) found that the jamming concentration can be simply expressed as $\phi_J = m\phi_{RCP}/(1-\phi_{RCP}+m\phi_{RCP})$ with $m = R_3\ R_1/R_2^2$ and ϕ_{RCP} the random close packing fraction, where R_k is the k^{th} moment of droplet size distribution. For example, if the droplet size is described by the Schulz distribution with $R_w/R_n = 2.0$ ($R_w = R_2/R_1$ and $R_n = R_1$), the jamming concentration becomes 0.725. It corresponds to a 5% increase of inter-droplets surface distance according to $h = 2a\phi_J^{1/3}\left(\phi^{-1/3}-(1-\alpha\gamma^2)^{-1/3}\right)$, which may slightly affect the value of the fitting parameter β in Eq. (2).

Flow curves collapse

Having addressed the role of long-range interaction on the emergence of solid-like behavior below ϕ_J and multiple scaling regimes above ϕ_J, we now probe its role on the solid-liquid transition under both steady shear and oscillatory shear. For simple jammed systems with only short-range repulsive interaction, the steady-state flow curves can be rescaled using the power laws for yield stress and characteristic time and collapsed onto a master curve above

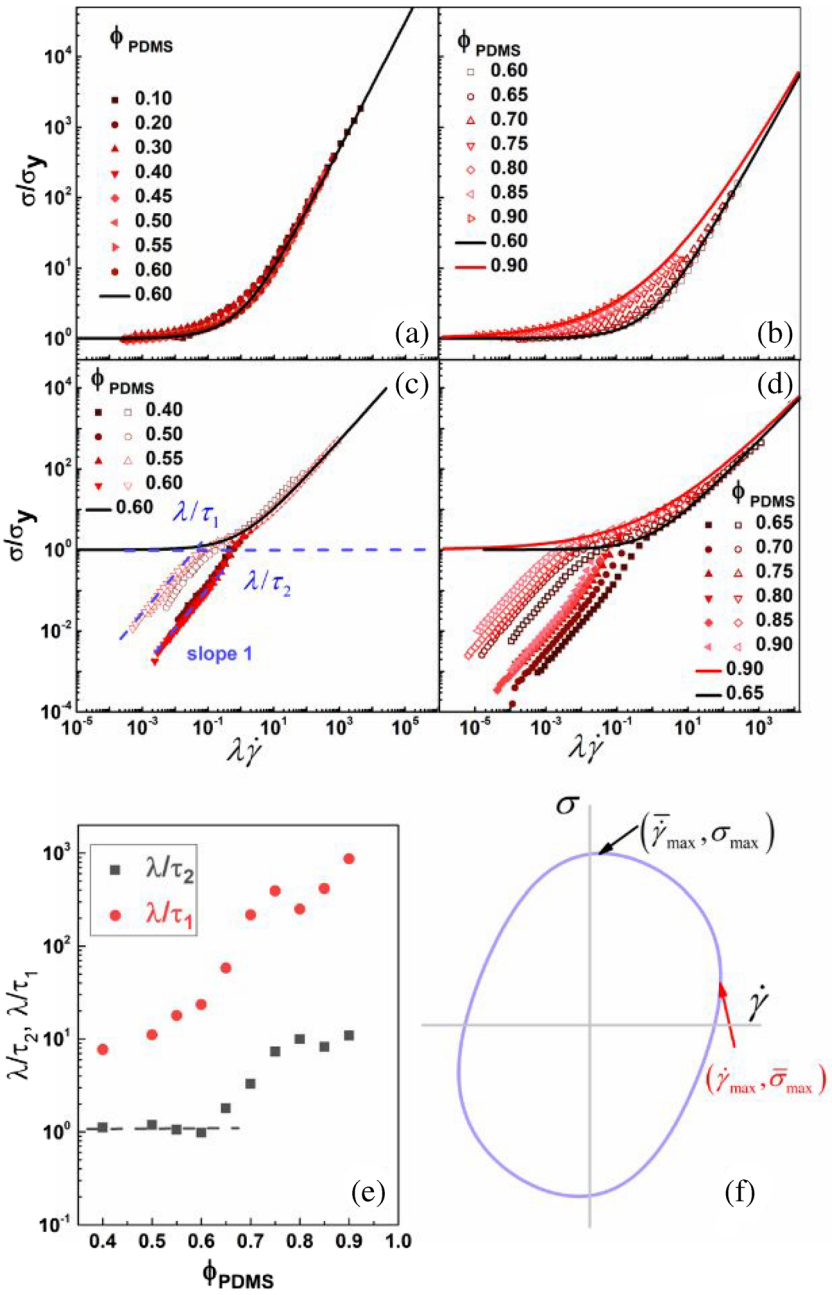

Fig. 7 Reduced stress ~ strain rate relation for steady flow curves (**a**, **b**) and dynamic flow curves from LAOS (**c**, **d**) below (**a**, **c**) and above (**b**, **d**) the jamming concentration. In (**c**) and (**d**), solid symbols denote the inter-cycle mean stress ~ strain rate relation$\sigma_{max}\sim\dot{\gamma}_{max}$.), and hollow symbols denote the inter-cycle stress ~ mean strain rate relation ($\sigma_{max}\sim\dot{\gamma}_{max}$). The relative relaxation times are shown in (**e**). The definition of the inter-cycle dynamic flow curves from the viscous Lissajous plots is shown in (**f**)

ϕ_J (Dekker et al. 2018; Dinkgreve et al. 2018, 2015; Paredes et al. 2013). Because such simple scaling relations do not exist due to the simultaneous contributions of the interfacial energy and the Frank elastic energy above jamming (Fig. 6), the steady shear stress is normalized by the apparent yield stress, and shear rate is normalized by the characteristic time. The normalized steady flow curves are shown in two groups in Fig. 7a and b for $\phi < \phi_J$ and $\phi > \phi_J$, respectively. It is seen that all steady flow curves collapse onto one master curve below ϕ_J, but the superposition failed aboveϕ_J. The failure of superposition above ϕ_J is clearly seen in the transition region from the solid-like regime at low shear rates and liquid-like regime at high shear rates. Note that collapsing of flow curves can only be obtained when there is one kind of interaction, either long-range repulsive interaction in PDMS/8CB emulsion below jamming or short-range repulsive interaction in normal emulsion above jamming. However, flow curves cannot collapse on master curves when short-range and long-range repulsive interactions contribute simultaneously above jamming transition, as in PDMS/8CB emulsions.

The solid-to liquid transition of a yield stress material can also be inferred by large amplitude strain sweep (LAOS) (Dagois-Bohy et al. 2017; Rogers et al. 2011; Rogers and Lettinga 2012; Yang et al. 2018; Yang and Yu 2017). The rescaling behavior of flow curves is further

probed in oscillatory shear with LAOS. To reveal the solid-liquid transition, we define two stress-strain rate curves from LAOS. For LAOS under controlled strain, two maximum points of viscous Lissajous curve ($\sigma\sim\dot{\gamma}$) at each strain amplitude can be identified at maximum strain rate and at maximum stress, respectively (Fig. 7f). These maximum points at different strain amplitude constitute the inter-cycle dynamic flow curves, $\sigma_{max}\sim\dot{\gamma}_{max}$ and $\sigma_{max}\sim\gamma_{max}$. Actually, two maximum points are the end points of two the geometric averages of the viscous Lissajous curve ($\sigma\sim\dot{\gamma}$), i.e., average shear stress versus strain rate curve $\sigma\sim\dot{\gamma}$ at constant strain rate and shear stress versus average strain rate $\sigma\sim\dot{\gamma}$ at constant shear stress (Yang et al. 2018). Such definition can also be used in LAOS under controlled stress condition. We would stress that only inter-cycle dynamic flow curves instead of the intra-cycle average curves were used to represent the transition, because the inter-cycle flow curves represent the maximum extent of transition under oscillatory shear at a specific strain amplitude or stress amplitude. As shown in Fig. 7c and d, the dynamic flow curves $\sigma_{max}\sim\dot{\gamma}_{max}$ and $\sigma_{max}\sim\dot{\gamma}_{max}$. superpose at high strain rate and bifurcate at low strain rate, where the bifurcation stress is regarded as the end of yield transition under LAOS (Yang et al. 2018). For PDMS/8CB emulsions below ϕ_J (Fig. 7c), the normalized dynamic flow curves $\sigma_{max}\sim\dot{\gamma}_{max}$ collapse in the whole range of strain rate while the failure of collapse appears below the bifurcation point of dynamic flow curves $\sigma_{max}\sim\dot{\gamma}_{max}$. Above ϕ_J, however, failure of collapse appears both above and below the bifurcation point of dynamic flow curves (Fig. 7d). In both cases, the dynamic flow curves above the bifurcation point are superposed on the corresponding steady flow curves. Below the bifurcation point, whether the dynamic flow curves can collapse rely on the composition dependence of the relaxation process in the solid-like state, i.e., when the shear stress is far below the yield stress. We define two characteristic times, τ_1 and τ_2, from the reciprocal of the crossover strain rate between the extrapolation of the linear stress-strain rate relation and the yield stress (Fig. 7c). As seen from the dependence of the time ratios (τ_1/λ and τ_2/λ) on composition (Fig. 7e), it is clear that the relative characteristic times τ_2/λ almost keep constant below ϕ_J ensuring the collapse of dynamic flow curves $\sigma_{max}\sim\dot{\gamma}_{max}$. However, the relative characteristic times τ_1/λ increase weakly with PDMS contents below ϕ_J, inducing weak failure of superposition for dynamic flow curves $\sigma_{max}\sim\dot{\gamma}_{max}$. Above ϕ_J, both time ratios increase significantly with PDMS content, leading to a larger distance between the dynamic flow curves below the yield stress especially for the $\sigma_{max}\sim\dot{\gamma}_{max}$ curve because of the larger value of τ_1/λ. The rescaling of dynamic flow curves under LAOS further validates that the type of interaction determines whether the flow curves can collapse.

Conclusions

In summary, we studied the solid-like behavior of PDMS/8CB emulsion, which emerges not only above the jamming concentration but also at low PDMS content. The solid-like behavior below jamming was ascribed to the long-range interaction between droplets. The long-range interaction changes from attractive at a larger inter-droplet distance when the PDMS content is low, to repulsive at a smaller inter-droplet distance when the PDMS content is above 0.2. In contrast to the short-range repulsive interaction, the long-range repulsive interaction can trap the non-colloidal droplets and induce yield stress at droplet fraction far below the jamming concentration. Meanwhile, simple power-law is not observed for yield stress and characteristic time above the jamming concentration because of the simultaneous contributions of long-range interaction and short-range repulsive interaction. Besides, the flow behaviors depend strongly on the type of interactions. Master curves of rescaled steady and dynamic curves can only be obtained when there is one kind of interaction, either long-range repulsive interaction in PDMS/8CB emulsion below jamming or short-range repulsive interaction in normal emulsion above jamming. Simple power-law scalings of yield stress and characteristic time are not the necessary condition to produce the master flow curves.

Funding This study received support from the National Natural Science Foundation of China (No. 51625303, 21790344).

References

Anderson VJ, Terentjev EM, Meeker SP, Crain J, Poon WCK (2001) Cellular solid behaviour of liquid crystal colloids 1. Phase separation and morphology. Eur Phys J E 4:11–20

Basu A, Xu Y, Still T, Arratia PE, Zhang Z, Nordstrom KN, Rieser JM, Gollub JP, Durian DJ, Yodh AG (2014) Rheology of soft colloids across the onset of rigidity: scaling behavior, thermal, and non-thermal responses. Soft Matter 10:3027–3035

Bécu L, Manneville S, Colin A (2006) Yielding and flow in adhesive and nonadhesive concentrated emulsions. Phys Rev Lett 96:138302

Berthier L, Biroli G (2011) Theoretical perspective on the glass transition and amorphous materials. Rev Mod Phys 83:587–645

Berthier L, Tarjus G (2009) Nonperturbative effect of attractive forces in viscous liquids. Phys Rev Lett 103:170601

Berthier L, Tarjus G (2011) The role of attractive forces in viscous liquids. J Chem Phys 134:214503

Bonn D, Denn MM, Berthier L, Divoux T, Manneville S (2017) Yield stress materials in soft condensed matter. Rev Mod Phys 89:035005

Boyd J, Buick JM, Green S (2007) Analysis of the Casson and Carreau-Yasuda non-Newtonian blood models in steady and oscillatory flows using the lattice Boltzmann method. Phys Fluids 19:093103

Bukusoglu E, Pal SK, de Pablo JJ, Abbott NL (2014) Colloid-in-liquid crystal gels formed via spinodal decomposition. Soft Matter 10:1602–1610

Chaudhuri P, Berthier L, Bocquet L (2012) Inhomogeneous shear flows in soft jammed materials with tunable attractive forces. Phys Rev E 85:021503
Chen DTN, Wen Q, Janmey PA, Crocker JC, Yodh AG (2010) Rheology of soft materials. Annu Rev Conden Matt Phys 1:301–322
Chuang I, ., Durrer R, ., Turok N, ., Yurke B, . (1991) Cosmology in the laboratory: defect dynamics in liquid crystals. Science 251: 1336–1342
Cohen-Addad S, Hohler R (2014) Rheology of foams and highly concentrated emulsions. Curr Opin Colloid In 19:536–548
Dagois-Bohy S, Somfai E, Tighe BP, van Hecke M (2017) Softening and yielding of soft glassy materials. Soft Matter 13:9036–9045
Dekker RI, Dinkgreve M, de Cagny H, Koeze DJ, Tighe BP, Bonn D (2018) Scaling of flow curves: comparison between experiments and simulations. J Non-Newton Fluid 261:33–37
Dinkgreve M, Paredes J, Michels MAJ, Bonn D (2015) Universal rescaling of flow curves for yield-stress fluids close to jamming. Phys Rev E 92:012305
Dinkgreve M, Michels MAJ, Mason TG, Bonn D (2018) Crossover between athermal jamming and the thermal glass transition of suspensions. Phys Rev Lett 121:228001
Divoux T, Grenard V, Manneville S (2013) Rheological hysteresis in soft glassy materials. Phys Rev Lett 110:018304
Fall A, Paredes J, Bonn D (2010) Yielding and shear banding in soft glassy materials. Phys Rev Lett 105:225502
Frank FC (1958) I. Liquid crystals. On the theory of liquid crystals. Discussions of the Faraday Society 25:19–28
Gam S, Meth JS, Zane SG, Chi C, Wood BA, Winey KI, Clarke N, Composto RJ (2012) Polymer diffusion in a polymer nanocomposite: effect of nanoparticle size and polydispersity. Soft Matter 8: 6512–6520
Hao B, Yu W (2019) A new solid-like state for liquid/liquid/particle mixtures with bicontinuous morphology of concentrated emulsion and concentrated suspension. Langmuir 35:9529–9537
He Q, Yu W, Wu YJ, Zhou CX (2012) Shear induced phase inversion of dilute smectic liquid crystal/polymer blends. Soft Matter 8: 2992–3001
Humpert A, Brown SF, Allen MP (2018) Molecular simulations of entangled defect structures around nanoparticles in nematic liquid crystals. Liq Cryst 45:59–69
Ikeda A, Berthier L, Sollich P (2013) Disentangling glass and jamming physics in the rheology of soft materials. Soft Matter 9:7669–7683
Irani E, Chaudhuri P, Heussinger C (2014) Impact of attractive interactions on the rheology of dense athermal particles. Phys Rev Lett 112:188303
Irani E, Chaudhuri P, Heussinger C (2016) Athermal rheology of weakly attractive soft particles. Phys Rev E 94:052608
Joshi YM (2014) Dynamics of colloidal glasses and gels. Annu Rev Chem Biomol 5:181–202
Katgert G, Tighe BP, van Hecke M (2013) The jamming perspective on wet foams. Soft Matter 9:9739–9746
Kawasaki T, Coslovich D, Ikeda A, Berthier L (2015) Diverging viscosity and soft granular rheology in non-Brownian suspensions. Phys Rev E 91:012203
Kim HS, Scheffold F, Mason TG (2016) Entropic, electrostatic, and interfacial regimes in concentrated disordered ionic emulsions. Rheol Acta 55:1–15
Koumakis N, Petekidis G (2011) Two step yielding in attractive colloids: transition from gels to attractive glasses. Soft Matter 7:2456–2470
Lidon P, Villa L, Manneville S (2017) Power-law creep and residual stresses in a carbopol gel. Rheol Acta 56:307–323
Liu AJ, Nagel SR (2010) The jamming transition and the marginally jammed solid. Annu Rev Conden Matt Phys 1:347–369
Lu B, Torquato S (1992) Nearest-surface distribution functions for polydispersed particle systems. Phys Rev A 45:5530–5544
Lu PJ, Weitz DA (2013) Colloidal particles: crystals, glasses, and gels. Annu Rev Conden Matt Phys 4:217–233
Mason TG, Scheffold F (2014) Crossover between entropic and interfacial elasticity and osmotic pressure in uniform disordered emulsions. Soft Matter 10:7109–7116
Mason TG, Bibette J, Weitz DA (1995) Elasticity of compressed emulsions. Phys Rev Lett 75:2051–2054
Meeker SP, Poon WC, Crain J, Terentjev EM (2000) Colloid-liquid-crystal composites: an unusual soft solid. Phy Rev E 61:R6083–R6086
Moller P, Fall A, Chikkadi V, Derks D, Bonn D (2009) An attempt to categorize yield stress fluid behaviour. Phil Trans R Soc A 367: 5139–5155
Nelson AZ, Ewoldt RH (2017) Design of yield-stress fluids: a rheology-to-structure inverse problem. Soft Matter 13:7578–7594
Nordstrom KN, Verneuil E, Arratia PE, Basu A, Zhang Z, Yodh AG, Gollub JP, Durian DJ (2010) Microfluidic rheology of soft colloids above and below jamming. Phys Rev Lett 105:175701
Olsson P, Teitel S (2007) Critical scaling of shear viscosity at the jamming transition. Phys Rev Lett 99:178001
Paredes J, Michels MAJ, Bonn D (2013) Rheology across the zero-temperature jamming transition. Phys Rev Lett 111:015701
Petekidis G, Vlassopoulos D, Pusey PN (2004) Yielding and flow of sheared colloidal glasses. J Phys Condens Matter 16:S3955–S3963
Poulin P, Cabuil V, Weitz DA (1997) Direct measurement of colloidal forces in an anisotropic solvent. Phys Rev Lett 79:4862–4865
Pusey PN (2008) Colloidal glasses. J Phys Condens Matter 20:494202
Pusey PN, van Megen W (1986) Phase behaviour of concentrated suspensions of nearly hard colloidal spheres. Nature 320:340–342
Rogers SA, Lettinga MP (2012) A sequence of physical processes determined and quantified in large-amplitude oscillatory shear (LAOS): application to theoretical nonlinear models. J Rheol 56:1–25
Rogers SA, Erwin BM, Vlassopoulos D, Cloitre M (2011) A sequence of physical processes determined and quantified in LAOS: application to a yield stress fluid. J Rheol 55:435–458
Santos A, Yuste SB, de Haro ML, Odriozola G, Ogarko V (2014) Simple effective rule to estimate the jamming packing fraction of polydisperse hard spheres. Phys Rev E 89:040302(R)
Scheffold F, Wilking JN, Haberko J, Cardinaux F, Mason TG (2014) The jamming elasticity of emulsions stabilized by ionic surfactants. Soft Matter 10:5040–5044
Senyuk B, Puls O, Tovkach OM, Chernyshuk SB, Smalyukh II (2016) Hexadecapolar colloids. Nat Commun 7:10659
Seth JR, Lavanya M, Clémentine LC, Michel C, Bonnecaze RT (2011) A micromechanical model to predict the flow of soft particle glasses. Nat Mater 10:838–843
Smalyukh II (2018) Liquid crystal colloids. Annu Rev Conden Matt Phys 9:207–226
Smalyukh II, Chernyshuk S, Lev BI, Nych AB, Ognysta U, Nazarenko VG, Lavrentovich OD (2004) Ordered droplet structures at the liquid crystal surface and elastic-capillary colloidal interactions. Phys Rev Lett 93:117801
Vlassopoulos D, Cloitre M (2014) Tunable rheology of dense soft deformable colloids. Curr Opin Colloid In 19:561–574
Wilking JN, Mason TG (2007) Irreversible shear-induced vitrification of droplets into elastic nanoemulsions by extreme rupturing. Phys Rev E 75:041407
Wood TA, Lintuvuori JS, Schofield AB, Marenduzzo D, Poon WCK (2011) A self-quenched defect glass in a colloid-nematic liquid crystal composite. Science 334:79–83
Wu Y, Wei Y, Zhou C (2006) A study on interfacial tension between flexible polymer and liquid crystal. J Colloid Interface Sci 298: 889–898

Yang K, Yu W (2017) Dynamic wall slip behavior of yield stress fluids under large amplitude oscillatory shear. J Rheol 61:627–641

Yang K, Liu Z, Wang J, Yu W (2018) Stress bifurcation in large amplitude oscillatory shear of yield stress fluids. J Rheol 62:89–106

Zapotocky M, Ramos L, Poulin P, Lubensky TC, Weitz DA (1999) Particle-stabilized defect gel in cholesteric liquid crystals. Science 283:209–212

Zywocinski A, Picano F, Oswald P, Géminard JC (2000) Edge dislocation in a vertical smectic—a film: line tension versus temperature and film thickness near the nematic phase. Phys Rev E 62:8133–8140

Publisher's note Springer Nature remains neutral with regard to jurisdictional claims in published maps and institutional affiliations.